Identification of a Blue Photoluminescent Composite Material from a Combinatorial Library

Jingsong Wang, Young Yoo, Chen Gao, Ichiro Takeuchi, Xiaodong Sun, Hauyee Chang, X.-D. Xiang,* Peter G. Schultz*

A quaternary combinatorial masking strategy was used in conjunction with photolithography to generate compositionally diverse thin-film phosphor libraries containing 1024 different compositions on substrates 2.5 centimeters square. A parallel imaging system and scanning spectrophotometer were used to identify and characterize compositions in the library with interesting luminescent behavior. Optimal compositions were identified with the use of gradient libraries, in which the stoichiometry of a material was varied continuously. This process led to the identification of an efficient blue photoluminescent composite material, $Gd_3Ga_5O_{12}/SiO_2$. Experimental evidence suggests that luminescence in this material may arise from interfacial effects between SiO_2 and $Gd_3Ga_5O_{12}$.

There is considerable interest in the development of advanced luminescent materials for a variety of applications, including flat panel displays and x-ray imaging systems. The properties of these materials arise from complex interactions among the host structure, dopants, and various defects and interfaces, all of which are strongly dependent on composition (*1*). Consequently, combinatorial strategies, in which large libraries or collections of materials are synthesized, processed, and screened, might be expected to accelerate the identification and optimization of phosphors with enhanced properties. Since the first applications of the combinatorial approach to the materials discovery process (*2*), substantial progress has been made in developing more efficient methods for generating and screening complex libraries of materials (*3*–*6*). Here we apply these methods to the identification of a new blue photoluminescent (PL) composite material, $Gd_3Ga_5O_{12}/SiO_2$.

Combinatorial materials libraries, which are designed to explore large numbers of empirically or theoretically defined compositions, are synthesized by sequentially depositing thin-film precursors at different sites on a substrate, using a series of precisely positioned shadow masks. The efficiency with which this search can be carried out is dictated by the masking scheme. A quaternary combinatorial masking scheme was devised for the PL libraries that involves a series of n different masks, which successively subdivide the substrate into a series of self-similar patterns of quadrants (Fig. 1). The rth ($1 \leq r \leq n$) mask contains 4^{r-1} windows; each window exposes one-quarter of the area deposited with the preceding mask. Within each window is an array of 4^{n-r} gridded sample sites. Each mask is used in up to four sequential depositions; each time, the mask is rotated by 90°. This process produces 4^n different compositions with $4n$ deposition steps and can be used to efficiently survey materials consisting of up to n elemental components, where each component is selected from a group of (up to four) precursors. This approach represents a substantial improvement in our ability to screen large landscapes of diverse compositions in comparison to simple binary (*2*) or gradient masking techniques and should be applicable to many classes of materials.

Increases in the spatial density of distinct compositions that can be synthesized and screened in a given library also improve the effectiveness of any combinatorial search. Consequently, photolithographic lift-off methods rather than physical shadow masks (*2*) were used to generate the PL libraries described here. Photolithography is well suited for generating libraries containing a high density of sites because of its high spatial resolution and alignment accuracy. In this procedure, before each thin-film deposition step, photoresist is deposited and patterned, leaving behind open windows. After thin-film deposition, the remaining photoresist and the overlying film are lifted off with acetone, leaving behind films only in the open window regions.

These methods were used to generate a library of silicate and gallate host materials containing a number of different activators. This particular library is based on the observation that some silicate- and gallate-based phosphors with relatively small band gaps have properties desirable for display applications (*1*). Refractory single-crystal substrates are typically used to minimize substrate-sample reactions and, in some cases, to assist epitaxial growth of thin-film materials. However, because our interest is ultimately in materials suitable for Si water–compatible light-emitting devices for optoelectronics applications, single-crystal Si substrates were used in this study. Three identical libraries were made, each containing $4^5 = 1024$ sites. The well-characterized phosphor Zn_2SiO_4:Mn (*1*) was included in the library as a reference, because this material is Si-compatible and efficient luminescent thin films can be made quite reproducibly.

The libraries consist of individual sites 650 μm by 650 μm, spaced 100 μm apart, deposited on thermally oxidized Si substrates 2.5 cm square. The five masks illustrated in Fig. 1 were used to generate the libraries. The sequence of masking and precursor deposition was as follows A_1: Ga_2O_3 (355 nm); A_2: Ga_2O_3 (426 nm); A_3: SiO_2 (200 nm); A_4: SiO_2 (400 nm); D_1: CeO_2 (3.5 nm); D_2: EuF_3 (11.3 nm); D_3: Tb_4O_7 (9.2 nm); E_1: Ag (3.8 nm); E_2: TiO_2 (6.9 nm); E_3: Mn_3O_4 (5.8 nm); B_1: Gd_2O_3 (577 nm); B_2: ZnO (105 nm); B_3: ZnO (210 nm); C_1: Gd_2O_3 (359 nm); C_2: Y_2O_3 (330 nm); and C_3: Y_2O_3 (82.5 nm). The numbers in parentheses are film thicknesses, and the notation X_i represents a deposition step with mask X rotated $(i - 1)$ 90° counterclockwise relative to the position depicted in Fig. 1. The steps corresponding to B_4, C_4, D_4, and E_4 were omitted in order to include in the library compounds consisting of less than five elements in order to study

J. Wang, C. Gao, I. Takeuchi, X.-D. Xiang, Materials Sciences Division, Lawrence Berkeley National Laboratory, Berkeley, CA 94720, USA.
Y. Yoo, Department of Physics, University of California, Berkeley, CA 94720, USA.
X. Sun and H. Chang, Department of Chemistry, University of California, Berkeley, CA 94720, USA.
P. G. Schultz, Materials Sciences Division, Lawrence Berkeley National Laboratory, and Howard Hughes Medical Institute, Department of Chemistry, University of California, Berkeley, CA 94720, USA.

*To whom correspondence should be addressed. E-mail: xdxiang@lbl.gov (X.-D.X.) or PGSchultz@lbl.gov (P.G.S.).

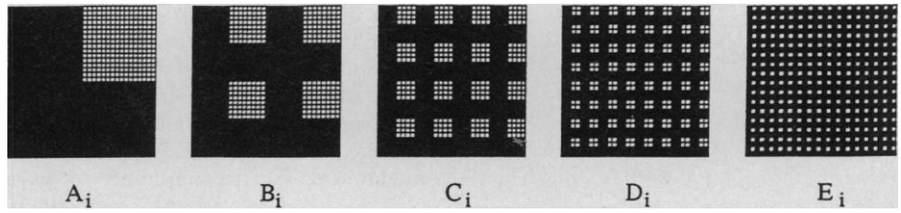

Fig. 1. Masks for generating the quaternary library. A_i, B_i, C_i, D_i, and E_i represent a deposition step with mask X rotated counterclockwise by $(i - 1) \times 90°$.

the effects of dopants. RF/DC sputtering and pulsed-laser deposition (PLD) were used for thin-film deposition, and targets of ≥99.95% purity were used. Profilometry studies revealed that the film thickness varied less than 5% over an area 2.5 cm in diameter. A photograph of the library under ambient light is shown in Fig. 2A.

Because the precursors are deposited on each site in a layered sequence, careful post-deposition annealing is required to ensure uniform diffusion of precursors and subsequent phase formation. Rutherford backscattering and x-ray diffraction (XRD) studies on a number of different films suggested that extended annealing at low temperatures (100° to 400°C) is often necessary before to high-temperature processing to ensure the formation of high-quality thin-film samples. This is especially true in the case of nonrefractive precursors, such as the silicates and gallates used here. Presumably, this low-temperature annealing procedure ensures uniform interdiffusion of precursors (*7*), prevents evaporation, and relieves mechanical stress. The library was therefore processed as follows: 200°C for >150 hours, 400°C for 24 hours, and 600°C for 12 hours, all in air; followed by treatment at 1000°C for 2 hours in a high-purity argon flow (with temperature ramping rates of 1°C per minute). In addition, the dopant precursors (EuF_3, CeO_2, Tb_4O_7, Ag, TiO_2, and Mn_3O_4) in the library were sandwiched by the host components to achieve better interdiffusion in the hosts. In this study, multiple identical libraries were generated in order to identify the optimal high-temperature processing conditions (processing under H_2 substantially reduced PL).

The PL photograph of the library (Fig. 2B) was taken under ultraviolet (UV) irradiation (centered around 254 nm). For more quantitative analysis of the libraries, a scanning spectrophotometer was used to measure the excitation and emission spectra of individual luminescent samples in the library. The emission and excitation spectra of approximately 100 selected bright blue, green, and red PL sites from the library were measured. By incorporating standard phosphors (Zn_2SiO_4:Mn) (*1*) in the library, one can obtain approximate relative photon outputs (Q) of each sample within the measured visible wavelength band. The Commission Internationale de l'Eclairage (CIE) color coordinates (*x*,*y*) and Q were calculated from the spectra (integrated from 400 to 675 nm) and are listed for a subset of the brightest samples (Table 1). The relative photon output of the blue site with nominal composition $Gd_{5.2}Ga_{3.33}O_z$ was calculated to be ~75% of the reference phosphor Zn_2SiO_4:$Mn_{0.05}$ (which has a quantum efficiency of 70%) (*1*). Optical effects in thin films complicate the direct determination of quantum efficiencies; however, if one assumes these effects are the same for both phosphors, an approximate quantum efficiency of ~50% can be estimated for the sample $Gd_{5.2}Ga_{3.33}O_z$. This is not as high as that of some commercial phosphors such as $BaMgAl_{10}O_{17}:Eu^{2+}$ [90% quantum efficiency (*1*)] but is substantially higher than that reported for porous silicon [1 to 10% quantum efficiency (*8*)].

Roughly 25 sites in the library showed substantial blue photoluminescence; all share the common precursors Gd_2O_3 and Ga_2O_3 (Fig. 2B). The brightest site, at which only these two precursors were deposited, corresponds to the nominal composition $Gd_{5.2}Ga_{3.33}O_z$. Bulk and thin-film samples on $LaAlO_3$ substrates with this nominal composition were made but showed no blue photoluminescence. We therefore suspected that the blue emission was related to the SiO_2 species that diffused into the host matrix from the Si substrate. To identify the optimal phosphor composition, we fabricated a square two-dimensional gradient library of composition $Gd_xGa_{1-x}O_z:(SiO_2)_y$, where the mole concentrations of Gd and Ga varied from 0 to 1 in the *x* direction, and the mole concentration of Si varied from 0.003 to 0.1 in the *y* direction. The gradient was generated with in situ, high-precision shutter masks in the PLD system. Two parallel shutter masks in close proximity to a mounted substrate were moved at a controlled speed from one end of the substrate to the other during deposition, resulting in a precise linear change in the thickness of the thin-film precursors. A (100)-oriented $LaAlO_3$ single crystal was used as the substrate, and SiO, Gd_2O_3, and Ga_2O_3 targets were used for PLD. After the same heat treatment used for the 1024 quaternary library, XRD studies were performed on different columns of the gradient library. For $x < 0.375$, only Ga_2O_3 and $Gd_3Ga_5O_{12}$ phases were identified; for $x > 0.375$, only $Gd_3Ga_5O_{12}$ and Gd_2O_3 phases were identified. The spectra of selected luminescent sample sites in the gradient library were measured. Generally speaking, the PL spectra consist of a broadband blue emission centered around 440 to 500 nm, similar to that observed for the blue PL sites in the library (Fig. 3A). The spectra have well-defined maxima with an energy spacing corresponding to 2100 cm^{-1}. The emission intensity as a function of *x* and *y* is shown in Fig. 3, B and C. The highest PL intensity corresponded to the composition $Gd_3Ga_5O_{12}/(SiO_2)_{0.08}$. Our XRD studies showed no trace of crystalline SiO_2 or silicate in $Gd_3Ga_5O_z:(SiO_2)_y$ ($y \leq 0.5$) bulk or thin-film samples. The possibility of bulk amorphous silicate is inconsistent with the observations that powder

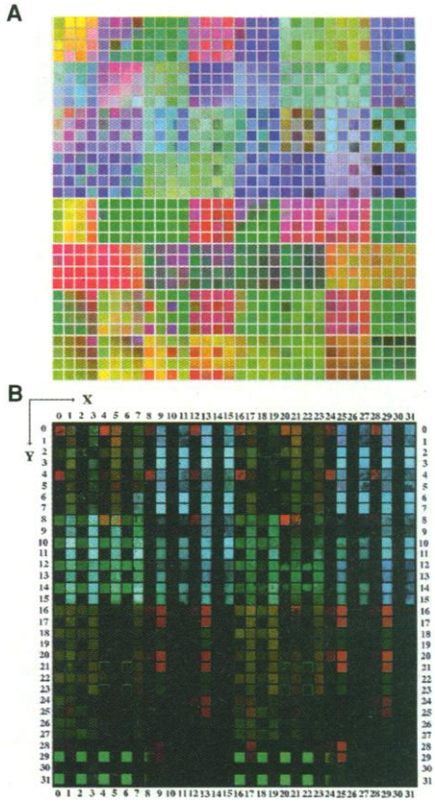

Fig. 2. (**A**) Photograph of the as-deposited quaternary library under ambient light. The diversity of colors in the different sites stems from variations in film thicknesses and the optical indices of refraction. (**B**) Luminescent photograph of the processed quaternary library under irradiation from a multiband emission UV lamp at short wavelength (centered around 254 nm).

Table 1. The CIE coordinates (*x*, *y*) and Q (in arbitrary units) of selected sample sites on the 1024 quaternary library.

Site (*x*, *y*)	Nominal composition	CIE (*x*, *y*)	Q
Green (20, 31)	$Zn_2SiO_4:Mn_{0.05}$	0.284, 0.672	1321
Blue (31, 3)	$Gd_{5.2}Ga_{3.33}O_z$	0.198, 0.236	994
Blue (15, 6)	$Gd_{3.2}Ga_4O_z:Ag_{0.05}$	0.184, 0.251	980
Blue (15, 7)	$Gd_{3.2}Ga_4O_z$	0.181, 0.246	915
Blue (15, 3)	$Gd_{5.2}Ga_4O_z$	0.179, 0.214	899
Blue (15, 2)	$Gd_{5.2}Ga_4O_z:Ag_{0.05}$	0.180, 0.214	827
Blue (31, 2)	$Gd_{5.2}Ga_{3.33}O_z:Ag_{0.05}$	0.195, 0.234	786

samples treated as above or at 1100°C for >32 hours showed no trace of crystalline silicate by XRD and have very weak luminescence (in contrast to the films), and the optimal stoichiometry coincides with $Gd_3Ga_5O_{12}$. However, x-ray photoemission spectroscopy (XPS) and energy-dispersive x-ray analysis confirmed the presence of SiO_2 in the sample. The measured percentage of SiO_2 in the sample was higher than that expected from the deposition stoichiometry, which suggests that SiO_2 is on the surfaces of the particles of $Gd_3Ga_5O_{12}$. XPS measurements also ruled out the presence of residual carbon in the sample. Consistent with these results, pure Gd_2O_3, Ga_2O_3 and $Gd_3Ga_5O_{12}$ thin films made on an $LaAlO_3$ substrate using the same procedures showed no PL in the same spectral region.

It is well known that both oxidized porous silicon (p-Si) (*9*, *10*) and properly prepared silicon oxide (*11*–*13*) show blue photoluminescence at 420 to 490 nm.

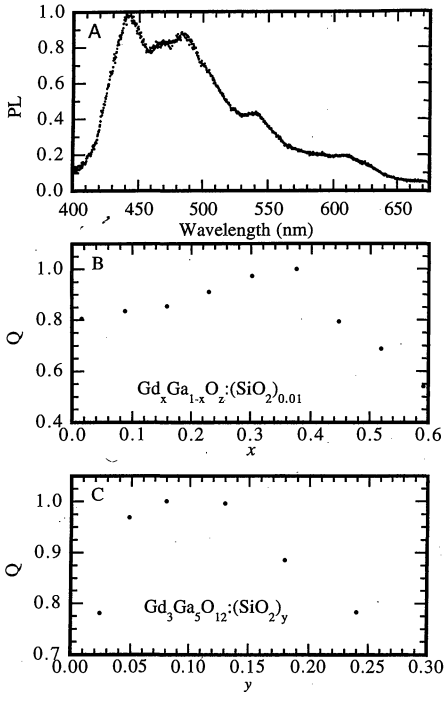

Fig. 3. (**A**) Photoluminescent spectrum of a sample site (31, 3) from the quaternary library [nominal composition $Gd_{5.2}Ga_{3.33}O_z$ under UV excitation at maximum wavelength (λ_{max}) (258 nm)]. (**B**) Photon output (Q) of $Gd_xGa_{1-x}O_z:(SiO_2)_{0.01}$ as a function of *x* under UV excitation at λ_{max} (256 nm). (**C**) Q of $Gd_3Ga_5O_{12}:(SiO_2)_y$ as a function of *y* under UV excitation at λ_{max} (256 nm). Spectra were measured with a scanning spectrophotometer consisting of a UV light source (a Xe lamp), a monochromator, a sample scanner, and a spectrograph. To increase data throughput, a liquid N_2-cooled charge-coupled-device camera was used to rapidly measure the spatially dispersed spectrum of each site (in seconds per sample). All scales are in arbitrary units.

Two models have been proposed to explain the blue PL from p-Si. The first model (*10*), used to explain the photoluminescence in SiO_x, connects the blue emission in p-Si directly to the defect states of SiO_2. In the second model [the extended quantum confinement (EQC) model], the PL arises from charge recombination processes across the broadened band gap of nanocrystalline Si (*14*). In our blue PL samples, the EQC model can be excluded because there is no pure Si in the sample. There are two possible origins for the blue PL in $Gd_3Ga_5O_{12}/SiO_2$. First, it is possible that Si may have substituted into the tetrahedral sites of Ga and functions as the activator in the host lattice of $Gd_3Ga_5O_{12}$. This notion is less likely because we are not aware of any report of Si-activated phosphors. It is more likely that nanocrystalline or amorphous SiO_2 or interfacial silicate (therefore not detectable by XRD) is finely dispersed into the $Gd_3Ga_5O_{12}$ matrix and possibly coated on the surface of $Gd_3Ga_5O_{12}$ grains, which are on the order of 100 nm as observed by atomic force microscopy. These interfaces may form the specific local electron states that give rise to the observed blue emission. Consistent with this notion, etching of the $Gd_3Ga_5O_{12}/SiO_2$ films with dilute hydrofluoric acid (which does not substantially affect the $Gd_3Ga_5O_{12}$ host) dramatically reduces photoluminescence in comparison to that in the untreated films. Additional experimental and theoretical investigations are needed to more fully understand the mechanism of luminescence in this material. Given the high PL efficiency and compatibility of the synthesis methods with Si wafer processing, this material may find applications in optoelectronics and imaging technologies.

REFERENCES AND NOTES

1. G. Blasse and B. C. Grabmaier, *Luminescent Materials* (Springer-Verlag, Berlin, 1994).
2. X.-D. Xiang *et al.*, *Science* **268**, 1738 (1995); G. Briceño, H. Chang, X. Sun, P. G. Schultz, X.-D. Xiang, *ibid.* **270**, 273 (1995).
3. E. Danielson *et al.*, *Nature* **389**, 944 (1997).
4. T. Wei, X.-D. Xiang, W. G. Wallace-Freedman, P. G. Schultz, X.-D. Xiang, *Appl. Phys. Lett.* **68**, 3506 (1996); H. Chang *et al.*, in preparation.
5. F. C. Moates *et al.*, *Ind. Eng. Chem. Res.* **35**, 4801 (1996).
6. X.-D. Sun *et al.*, *Adv. Mater.* **9**, 1046 (1997).
7. L. Fister, T. Novet, C. A. Grant, D. C. Johnson, *Advances in the Synthesis and Reactivity of the Solids* (JAI, New York, 1994), vol. 2, pp. 155–234.
8. R. T. Collins, P. M. Fauchet, M. A. Tischler, *Phys. Today* **50**, 24 (1997).
9. T. Ito, T. Ohta, A. Hiraki, *Jpn. J. Appl. Phys.* **31**, L1 (1992).
10. L. Tsybeskov, Ju. V. Vandyshev, P. M. Fauchet, *Phys. Rev. B* **49**, 7821 (1994).
11. J. H. Stathis and M. A. Kastener, *ibid.* **35**, 2972 (1987).
12. R. Tohmon *et al.*, *Phys. Rev. Lett.* **62**, 1388 (1989); H. Nishikawa, T. Shiroyma, R. Nakamura, Y. Ohki, *Phys. Rev. B* **45**, 586 (1992).
13. G. G. Qin *et al.*, *Phys. Rev. B* **55**, 12876 (1997).
14. F. Koch, in *Materials Research Society Symposia Proceedings No. 298*, M. A. Tischler, R. T. Collins, M. L. Thewalt, G. Abstreiter, Eds. (Materials Research Society, Pittsburgh, PA, 1993), p. 319.

15. We thank W. D. Hinsberg for helpful advice. This work was supported by the Office of Naval Research; by the Director, Office of Energy Research, Office of Basic Energy Research, Division of Materials Sciences, of the U.S. Department of Energy; and by the W. M. Keck foundation.

13 November 1997; accepted 2 February 1998

Cortical Map Reorganization Enabled by Nucleus Basalis Activity

Michael P. Kilgard* and Michael M. Merzenich

Little is known about the mechanisms that allow the cortex to selectively improve the neural representations of behaviorally important stimuli while ignoring irrelevant stimuli. Diffuse neuromodulatory systems may facilitate cortical plasticity by acting as teachers to mark important stimuli. This study demonstrates that episodic electrical stimulation of the nucleus basalis, paired with an auditory stimulus, results in a massive progressive reorganization of the primary auditory cortex in the adult rat. Receptive field sizes can be narrowed, broadened, or left unaltered depending on specific parameters of the acoustic stimulus paired with nucleus basalis activation. This differential plasticity parallels the receptive field remodeling that results from different types of behavioral training. This result suggests that input characteristics may be able to drive appropriate alterations of receptive fields independently of explicit knowledge of the task. These findings also suggest that the basal forebrain plays an active instructional role in representational plasticity.

The mammalian cerebral cortex is a highly sophisticated self-organizing system (*1*). The statistics of sensory inputs from the external world are not sufficient to guide cortical self-organization, because the behavioral importance of inputs is not strongly correlated with their frequency of occurrence. The behavioral value of stimuli has been shown to